Effects of the energy spread of secondary electrons in a dc-biased single-surface multipactor

Min Sup Hur, Jung-Il Kim, Geun-Ju Kim, and Seok-Gy Jeon

Citation: Phys. Plasmas **18**, 033103 (2011); doi: 10.1063/1.3561786
View online: http://dx.doi.org/10.1063/1.3561786
View Table of Contents: http://pop.aip.org/resource/1/PHPAEN/v18/i3
Published by the AIP Publishing LLC.

Effects of the energy spread of secondary electrons in a dc-biased single-surface multipactor

Min Sup Hur,[1] Jung-Il Kim,[2] Geun-Ju Kim,[2] and Seok-Gy Jeon[2,a)]
[1]*UNIST, BanYeon-Ri 100, Ulju-gun, Ulsan 689-798, South Korea*
[2]*Center for Pioneering Medical-Physics Research, KERI, 1271-19 Sa-dong, Ansan-si 426-170, South Korea*

(Received 7 January 2011; accepted 11 February 2011; published online 8 March 2011)

The effects of the energy spread of secondary electrons are theoretically investigated for a dc-biased single-surface multipactor. In our previous publication [S. G. Jeon *et al.*, Phys. Plasmas **16**, 073101 (2009)], we obtained the conditions for the phase lock of an electron bunch, assuming zero velocity spread of the secondary electrons. In this work, we extended our previous theory to derive a quadratic map, by which the stability and bifurcation of the electron bunch can be systematically investigated. For the study of the energy spread of the secondary electrons, a randomized term was added to this map. The modified map then showed significant smearing-out of the bifurcated branches. The theoretical results were verified by particle-in-cell simulations, which showed good agreement in wide parameter ranges for both cases of monoenergetic and energy-spread secondary electrons. © *2011 American Institute of Physics*. [doi:10.1063/1.3561786]

I. INTRODUCTION

The multipactor discharge is a commonly observed phenomenon in the high power microwave systems.[1] This is an electron avalanche resonantly driven by the coupling of the secondary electron emission and rf field: Some initial free electrons merely existing in the vacuum are accelerated by the rf field to hit a dielectric or conducting surface energetically to yield secondary electrons. Then the emitted electrons return to the surface after a few rf cycles and hit it again yielding another secondary electrons. The reason why such a process leads to the electron avalanche is that the secondary yield, i.e., number of emitted electrons for a given incident electron, is usually larger than unity in most of the rf device regimes.

In most rf devices, the multipactor discharge is usually considered as something to be suppressed since the rapidly proliferating electrons can seriously damage the surface, dissipate microwave energy, change the cutoff conditions of the microwave transmission, and sometimes even lead to the vacuum breakdown.[1–3] In that context, there have been decades of intensive research to suppress the multipactor discharge: for example, the treatment of the surface to reduce the secondary emission yield,[4,5] changing the design of the rf tube, or fabricating the surface structure[6,7] to lead the emitted electrons in the other way.

While most of the research has been devoted to mitigating the multipactor, there has been another stream of research to utilize it actively for the generation of well-sliced electron bunches.[8,9] Because the multipactor is an avalanche procedure, it is possible to make highly intense cold electron beams if certain resonance conditions are satisfied. One of the most suitable designs for this purpose may be the dc-biased single-surface multipactor, where both dc and ac fields are perpendicular to the emission surface. In this geometry, since the electrons are emitted in one side only, the other open side can be used easily for the installation of the beam extraction plate without disturbing the bunch generation process. The normal dc field helps push back the electrons onto the emission surface. When certain conditions are satisfied, the returning electrons lead to larger-than-unity yield of the secondary electrons. As is to be seen later, the dc field is quite important to the generation of stable (actually proliferating) single bunches of the electrons.

Because of such an unusual configuration, which is very rare in generic rf systems, there have been just a few studies on the dc-biased single-surface multipactors.[10,11] In those works, they found the equation of the fixed point, which represents the initial phase of such an electron that when it returns to the target (emission surface), the rf phase becomes the same as that at the moment of its emission. That is, when an electron with the initial phase θ_0 returns and hits the target, the next secondary electron is also emitted with θ_0. The primary interest in those previous contexts, especially Ref. 11, was to find the resonance zones for the single-bunched multipacting as functions of the secondary emission velocity. Furthermore, Semenov *et al.*[11] reported the observation of the multiphase regimes from the numerical calculation of the single-electron equation. In the multiphase regime, the phase of the emitted electrons oscillates between multiple values instead of converging to a single fixed point. Typically, they show two, four, and stochastic oscillations as the dc bias changes. The multiphase feature was addressed again in our recent work,[12] where we found a parameter map showing the transition (bifurcation) from the single fixed point to double fixed points.

In a practical point of view, it is difficult to dc-bias the rf resonator in a high frequency regime like tens of gigahertz since the usage of the insulating gap to sustain the dc field usually deteriorates significantly the quality factor of the resonator. In our previous work,[12] we suggested using a photonic crystal structure to solve this problem. Motivated by the experimental plan of such a suggestion, in the same pa-

a)Electronic mail: sgjeon72@keri.re.kr.

per, we addressed theoretically the dc-biased multipactor on a single surface. The starting point was the surprisingly simple single-electron equation of motion, with the space charge effect neglected. First we derived the equation of the fixed point θ_0 and the stability condition of that point, similarly as in Refs. 10 and 11. Since all other electrons which do not satisfy the fixed point condition disappear by being absorbed on the target, a single bunch of electrons can be generated. Second we established the stability condition of the fixed point in terms of the dc and ac fields. By numerically solving the single-electron equation, we observed up to the first bifurcation (i.e., the transition into the multiphase) of the fixed point. The bifurcation of the fixed point results in the double bunches of the electrons in the real space, which was verified by a particle-in-cell (PIC) simulation. Similar analysis about the fixed point and its bifurcation for double-surface dc-biased multipactor can be found in Ref. 13.

In our previous analysis of the stability and bifurcation,[12] it was assumed that the emission velocity of the secondary electron was negligible. However, in the real surface, the electrons are usually emitted with non-negligible energies. Furthermore, there is significant energy spread in the emission energy spectrum. The primary goal of the present work is investigating the effects of the energy spread on the stability and property of the single or multiple electron bunches. We started from the same single particle equation as before, neglecting the energy spread (but keeping the general non-zero emission velocity). But this time we addressed the stability and bifurcation issues by finding a quadratic mapping function of the phase perturbation. From the analysis of the mapping function the theoretical conditions of the first and second bifurcations were obtained. Then the mapping function was modified to include the emission energy spread. It was found that the original bifurcation diagram was qualitatively preserved, but high-order branches were merged to each other by the energy spread. The bifurcation diagram was verified by PIC simulations for both monoenergetic and energy-spread cases, which showed good agreement for wide ranges of parameters.

The mapping function approach is advantageous in addressing the multiphase issues. In Ref. 11, the transition (bifurcation) to the multiphase was observed from direct numerical integration of the single-electron equation. However, by using the mapping function as in this present work, the parameter regimes for single, double, quadruplet, and stochastic oscillations of the fixed point can be investigated more systematically without integrating the equation of motion. Furthermore, we explored the bifurcation as a function of control parameters, such as dc or ac amplitude, instead of the intrinsic parameter such as the emission velocity.[11] Implementation of the secondary energy spread into the mapping model is also a unique point of the present work.

This paper is organized as follows. In Sec. II, the mapping theory of stability and bifurcation of the fixed point is presented along with the PIC simulation results. In Sec. III, the modified mapping function is presented for the energy spread and compared with the PIC simulations. We summarize our major conclusions in Sec. IV.

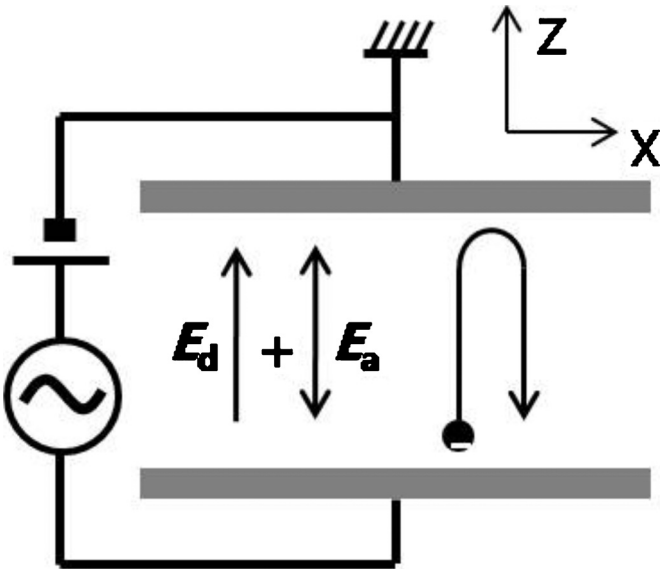

FIG. 1. The schematics of the multipactor system. Two parallel plates are driven by the combined dc and ac fields. In a real system the ac field is provided by the radio-frequency wave in a photonic crystal structure (Ref. 12). Only the lower plate yields the secondary electrons. The upper plate absorbs the electrons in the simulation.

II. FIXED POINT THEORY WITH ZERO VELOCITY SPREAD OF THE SECONDARY ELECTRONS

A. Fixed point equation

When the space charge effect and the radiation by electron motion are neglected, the electrons interact only with the applied dc and ac electric fields. Thus, the single-electron equation of motion is just enough to understand the system:

$$\frac{d^2z}{dt^2} = -\frac{e}{m}E_d - \frac{e}{m}E_a \sin(\omega t + \theta_0), \tag{1}$$

where E_a is the amplitude of the ac electric field and E_d is the dc electric field. In the system arranged as in Fig. 1, E_d is aligned in the positive z-direction, so that the electrons can impact on the emission plate strong enough to yield numerous secondary electrons. However, E_a should be sufficiently larger than E_d to prevent premature impact.[12] The integration of Eq. (1) by time yields the velocity and the position of a single electron:

$$v(t) = v_0 - \frac{eE_d}{m}t + \frac{eE_a}{m\omega}[\cos(\omega t + \theta_0) - \cos\ \theta_0], \tag{2}$$

$$z(t) = \left(v_0 - \frac{eE_a}{m\omega}\cos\ \theta_0\right)t - \frac{eE_d}{2m}t^2 + \frac{eE_a}{m\omega^2} \times[\sin(\omega t + \theta_0) - \sin\ \theta_0]. \tag{3}$$

Note that the electron starts from $z=0$ at $t=0$ with the initial velocity v_0 in Eq. (3).

The resonance condition can be defined such that the emitted electron returns to its original position after the nth period of the ac field, so that the next electrons (i.e., by the secondary emission with v_0) start from exactly the identical condition as their parent electrons. Then for the resonance, $z(t=2n\pi/\omega)=0$, which yields the fixed point equation

$$\cos\theta_0 = \frac{m\omega v_0}{eE_a} - n\pi\frac{E_d}{E_a}. \tag{4}$$

In other words, if an electron starts with the initial phase θ_0, then it returns to the original position with the phase θ_0 after n-oscillations of the ac field. For the convenience in calculation further on, the variables are normalized as follows.

$$\epsilon = \frac{E_d}{E_a}, \quad \nu = \frac{m\omega}{eE_a}v_0, \tag{5}$$

where ϵ and ν represent the ratio of the dc electric field to the ac amplitude and the normalized emission velocity of the secondary electron, respectively.

The possible range of $\cos\theta_0$ and $\sin\theta_0$ is restricted by a couple of conditions: First, the electron velocity at the moment of impact should be in the $-z$-direction and, second, the direction of the force just after the impact should be positive to prevent the premature impact. The first condition gives $v(\omega t = 2n\pi) < 0$ in Eq. (2), which yields, along with Eqs. (4) and (5),

$$\cos\theta_0 < \frac{\nu}{2}. \tag{6}$$

From the second condition and Eq. (1),

$$\sin\theta_0 < -\epsilon. \tag{7}$$

Inequality (7) indicates that $\sin\theta_0$ is always negative. From inequality (6), the maximum possible value of θ_0 is determined by $3\pi/2 + \arcsin(\nu/2)$. This is consistent with Eq. (6) in Ref. 11, except the shift by π, which originates from the different sign of the ac field in single-electron equation. Inequality (7) is valid only for zero emission velocity. For finite emission velocity, according to Ref. 11 (and considering the different sign of the ac field), the minimum possible phase is determined by $\pi + \arctan(1/n\pi - \sqrt{8\nu/3})$.

B. Stability of the fixed point

Here, we investigate the stability of the fixed point θ_0. If an electron starts with θ_0 satisfying Eq. (4), it always returns to the emission plate with exactly the same phase. Thus, the next emitted electron takes the identical path to its previous one, resulting in the periodic repetition of the emission and returning. However, in the real multipactor, the electrons can easily deviate from such a resonant trajectory by space charge effects, delay in the secondary emission, energy and angle spread of the secondary emission, etc. If the fixed point is stable, the deviated electrons can be attracted again to the fixed point. Such an attraction is possible because the multipactor system is not an energy-conserved one. Instead, some electron energies are always lost through the emission plate since the emission energy of the secondary electron does not have much correlation with the incident energy. Such a "damping" can lead to the stable attractor, i.e., the fixed point.

For the analysis we find the mapping from a small deviation Δ_k at the kth cycle to the deviation at the next cycle Δ_{k+1}. The deviation Δ_k is defined by $\Delta_k = \theta_k - \theta_0$, where θ_k is the initial phase relative to the ac field at the kth cycle. The time taken for the electron to return in the next cycle is denoted by $\tau = \omega t$, which is a function of the previous starting phase θ_k. The deviation at the next cycle, after the n oscillations of the ac field, is $\Delta_{k+1} = \theta_{k+1} - \theta_0 = \theta_k + \tau - \theta_0 - 2n\pi$. Note that $\tau(\theta_0) = 2n\pi$. Up to the second order of Δ's,

$$\frac{\Delta_{k+1}}{\Delta_k} = 1 + \frac{\tau(\theta_k) - \tau(\theta_0)}{\theta_k - \theta_0} \simeq 1 + \left.\frac{\partial\tau}{\partial\theta}\right|_{\theta_0} + \frac{\Delta_k}{2}\left.\frac{\partial^2\tau}{\partial\theta^2}\right|_{\theta_0}. \tag{8}$$

The derivatives $\partial_\theta\tau$ and $\partial_\theta^2\tau$ can be obtained from Eq. (3). After τ the electron returns to the emission plate, so $z(\tau) = 0$. Thus,

$$(\nu - \cos\theta_k)\tau - \tfrac{1}{2}\epsilon\tau^2 + \sin(\tau + \theta_k) - \sin\theta_k = 0. \tag{9}$$

The differentiation of Eq. (9) by θ_k and substituting $\theta_k = \theta_0$ yields

$$\tau_0' = -\frac{2n\pi\sin\theta_0}{\nu - 2n\pi\epsilon} = \frac{2n\pi\sqrt{1 - (\nu - n\pi\epsilon)^2}}{\nu - 2n\pi\epsilon}, \tag{10}$$

where the prime means the derivative in terms of θ and the subscript zero means that the derivative is evaluated at $\theta = \theta_0$. By differentiating once more Eq. (9), the second derivative of τ can be obtained:

$$\tau_0'' = \frac{2n\pi}{(\nu - 2n\pi\epsilon)^3}\{2n\pi[\epsilon - \sqrt{1 - (\nu - n\pi\epsilon)^2}^3] - (\nu - n\pi\epsilon) \times (\nu^2 - 2n\pi\epsilon\nu + 2n^2\pi^2\epsilon^2)\}. \tag{11}$$

If the mapping from Δ_k to Δ_{k+1} is written as $\Delta_{k+1} = f(\Delta_k)$, then from Eq. (8),

$$f(x) = x(b + ax), \tag{12}$$

where $b = 1 + \tau_0'$, $a = \tau_0''/2$, and τ_0' and τ_0'' are determined by Eqs. (10) and (11). The coefficients a and b are plotted as functions of ϵ in Fig. 2 for some typical ν's.

Using the mapping found above, the stability of the fixed point can be investigated. Just the $n = 1$ case is considered. The stability condition can be revealed by examining the equilibrium point (attractor) of the mapping $f(x)$, i.e., $f(x_0) = x_0$. When $|df(x_0)/dx| < 1$, x_0 is a stable equilibrium since any small perturbation from x_0 will be attracted to x_0 after several iterations. As seen from Fig. 2, the coefficients a and b are mostly negative for ϵ from 0.29 to 0.37, which is an interesting range since a stable single-electron bunch is generated there as will be shown later. Therefore, the mapping looks like that in Fig. 3 in this range. There are two equilibrium points: one is at $x_0 = 0$ and the other is at $x_0 = (1-b)/a = 2\tau_0'/\tau_0''$. For the latter it is obviously $|f'(x_0)| > 1$ (unstable). At $x_0 = 0$, $f'(0) = b$. Thus, the stability condition for the fixed point θ_0 is

$$|b| = \left|1 + \frac{2\pi\sqrt{1 - (\nu - \pi\epsilon)^2}}{\nu - 2\pi\epsilon}\right| < 1. \tag{13}$$

Note that the function $f(x)$ maps Δ_k to Δ_{k+1}. When the stability condition (13) is satisfied, any small Δ will converge to zero as the iteration goes on, which means that the electron phase relative to the ac field will converge to θ_0.

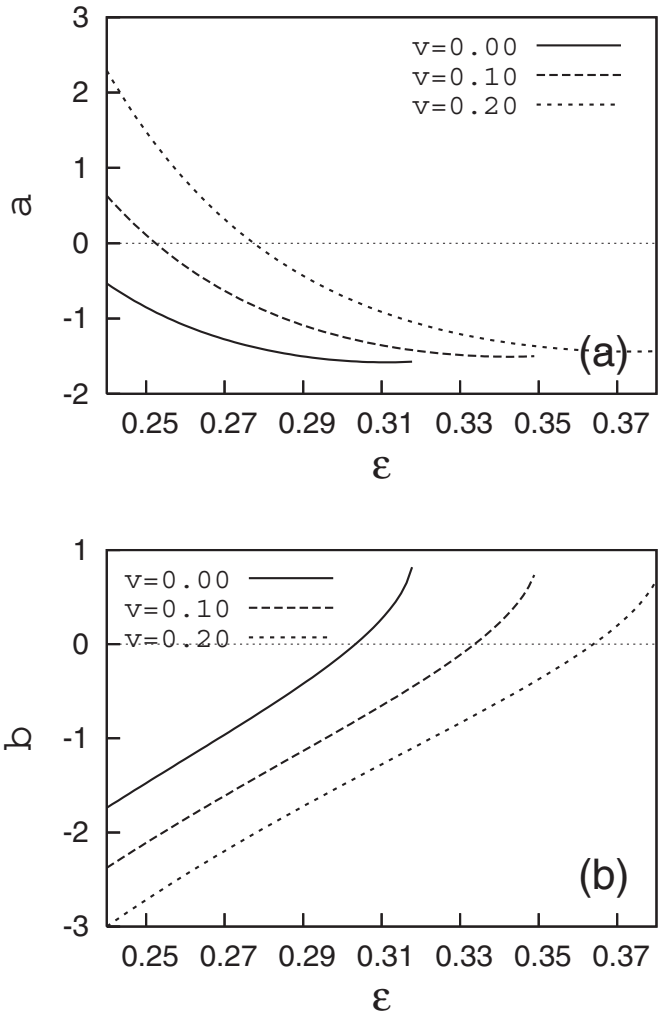

FIG. 2. The coefficients a and b in Eq. (12) for a typical range of ϵ.

C. Bifurcation of the fixed point

As seen in Fig. 2(b), $|b|=|f'(0)|$ can be increased beyond unity as ϵ is decreased. Beyond the stability breaking, cascading of bifurcations is expected as in the logistic map, because the mapping $f(x)$ is quadratic. Here, the meaning of the bifurcation is the splitting of a given fixed point branch in a parameter map into two or more multiple branches. Typically, as dc field decreases, the original single fixed point splits into two stable phases, and then each two phases split again into another two phases (so a total of four stable phases). Such a cascading process repeats to reach stochastic oscillations. For example, the first bifurcation can be explored by examining $f(f(x_n))=x_n$. Near the bifurcation, the coefficient b can be written by $b=-1-\delta$, where $0<\delta\ll 1$. And also the new equilibrium x_n is not much different from x_0, i.e., $|x_n|\ll 1$. Then from double iterations of Eq. (12), keeping up to the second order of δ and assuming $x_n\sim\sqrt{\delta}$, we obtain

$$x_n \simeq \frac{-1-b-4\sqrt{-1-b}}{4a}. \tag{14}$$

The leading order in Eq. (14) is $\sqrt{\delta}$, so the initial assumption $x_n\sim\sqrt{\delta}$ is verified. The slope of $F(x)=f(f(x))$ at x_n is, up to the order of $\delta\sqrt{\delta}$,

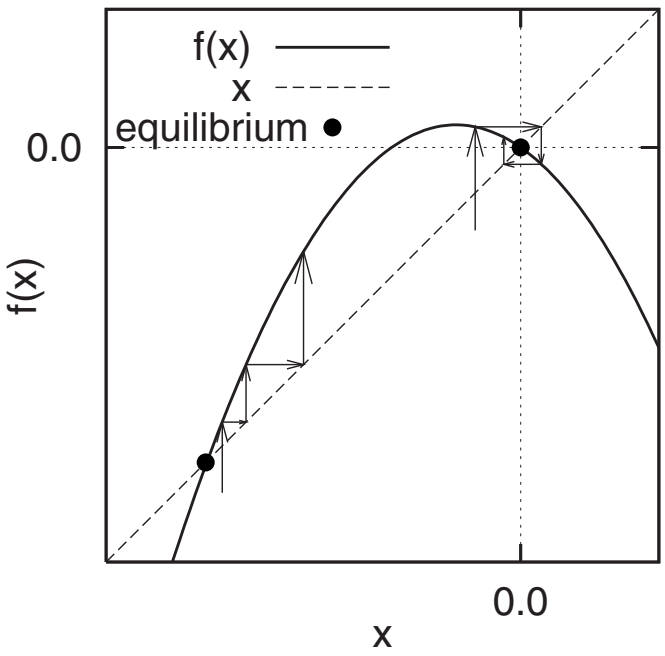

FIG. 3. Map from Δ_k to Δ_{k+1}. The filled circles represent the equilibrium points. At around the equilibrium $x=0$, the initial perturbation converges to zero. At around the other equilibrium, any arbitrary perturbation grows. The stability of $x=0$ depends on the slope of $f(x)$ there.

$$F'(x_n)=f'(f(x_n))f'(x_n)\simeq 5+4b+3(b+1)\sqrt{-1-b}. \tag{15}$$

Equation (15) is roughly $F'(x_n)\sim 5+4b$. Consequently, the stability condition of the two-period bifurcated state is

$$-1.5<b<-1. \tag{16}$$

In this bifurcated state, the phase of the electron (at the moment of impact on the emission plate) alternates between $x_n+\theta_0$ and $f(x_n)+\theta_0$, where

$$f(x_n)\simeq \frac{-3(1+b)+4\sqrt{-1-b}}{4a}. \tag{17}$$

Figure 4 shows the bifurcation diagrams of the fixed point θ_0, which were obtained from direct iterations of mapping (12). We plotted $\theta_k=\theta_0+\Delta_k$ instead of Δ itself. The dashed lines represent theoretical branches from Eqs. (14) and (17) (added by θ_0), which agree well with the direct iterations up to the second bifurcation points. Because the mapping is valid only for a small Δ, it is not exactly coincident with the PIC simulation results for a small ϵ, where Δ is large. Note that the discrepancy of the PIC from the mapping, especially near the first bifurcation points, originated partially from the space charge effect, which was not considered in the theory. When the space charge effect was toggled off, the PIC exactly overlapped on the theoretical curves near the first bifurcation points. Even though there is some discrepancy, the mapping still preserves well the qualitative behavior of the fixed points even in the small-ϵ region: for example, the four-branch bunching was observed in the PIC simulations as predicted by the mapping at $\epsilon=0.274$ for $\nu=0.1$ and $\epsilon=0.3$ for $\nu=0.2$. Figure 5 shows the PIC simu-

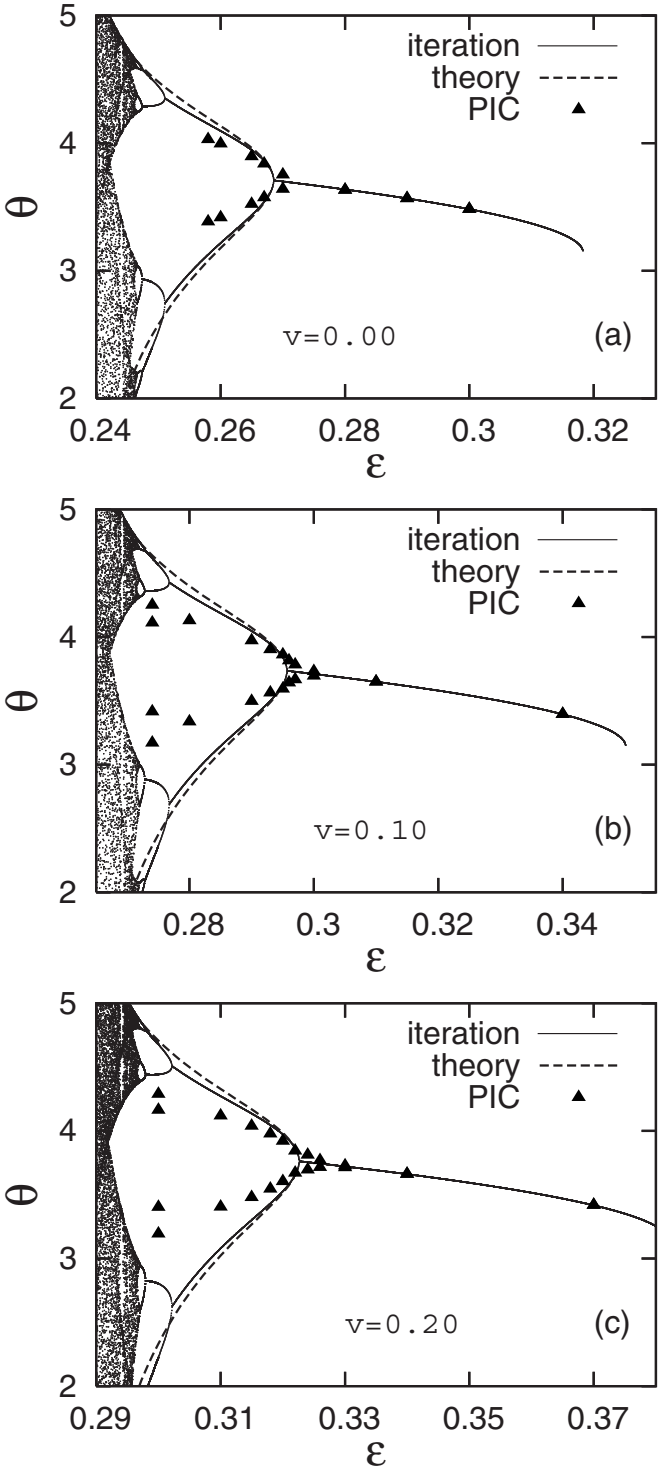

FIG. 4. Bifurcation diagrams for (a) ν=0, (b) ν=0.1, and (c) ν=0.2. The solid lines were obtained from direct iterations of the mapping equation (12), and the theoretical curves (dashed lines) were from Eqs. (14) and (17). The triangles represent the PIC simulation results.

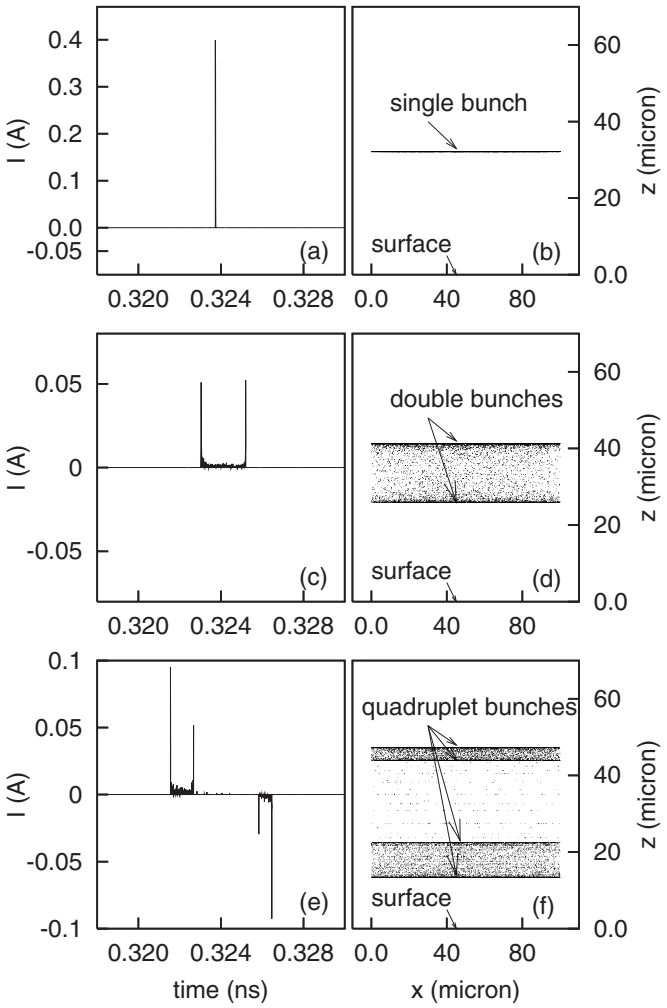

FIG. 5. The electric current measured at the target (left column) and the electron distribution in a real x-z space (right column) for ν=0.2. The electric current is the total charge flowing out of the system per unit time, so its sign is determined by the difference in the number of incident and emitted electrons. The electron distributions in the right column exhibit significant grouping into (b) single, (d) double, and (f) quadruplet bunches. The remnant electrons existing between the major bunches are possibly the nonsaturated ones or the resonant electrons with higher modes ($n>1$).

lations of the electric currents measured at the emission target and x-y phase space of the bunched electrons for single, double, and quadruplet bunching.

The accuracy of the stability condition (16) for the double bunching was found to be reasonably good. In Fig. 4, the values of ϵ at which the system transits from double bunch to the quadruplet bunch, i.e., the second bifurcation point, are 0.251, 0.277, and 0.302, respectively. The coefficient b for those ϵ's is -1.45 for all those three cases, which coincides well with Eq. (16).

It may be useful to describe the actual parameters used in the PIC simulations. The frequency and amplitude of the driving ac field were fixed at 35 GHz and 5.941 V/μm, respectively. For these parameters, the values of ν used here (0, 0.1, and 0.2) correspond to 0, 0.65, and 2.6 eV, respectively. These numbers for the emission energy of the secondary electrons are in the typical range of emission energy from copper, stainless steel, and other materials.[14] The dc field was varied to change ϵ. The simulations were two dimensional. The length of the target was 100 μm, which was divided by 20 meshes. The span in the z-direction in Fig. 1 was set large enough (70–300μm depending on the cases), and initially the electrons were loaded uniformly in the whole space to accommodate all possible initial phases of the initial electrons. Since the motion of the electrons is dominant in the

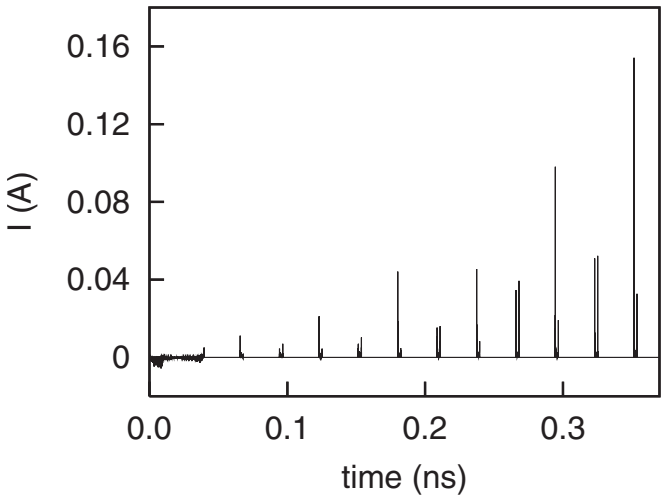

FIG. 6. The electric current in the whole time domain of the simulation for $\nu=0.10$ and $\epsilon=0.29$, which is the case of Figs. 5(c) and 5(d).

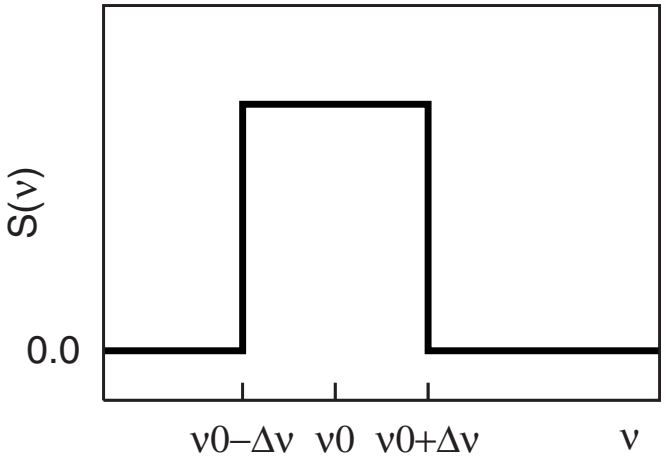

FIG. 7. The velocity spectrum of the secondary electrons assumed in the theory and simulations.

z-direction, it was resolved more finely by a 2 μm mesh. The simulation time step was 5 fs, which was small enough to satisfy the Courant condition. Initially the electrons were loaded uniformly in the whole domain, just some of which survived to satisfy the fixed point condition and to proliferate by the secondary emission. The fixed point could be determined in the simulation as follows. The system is driven by $\cos\omega t$ in the simulation, while the driving term in Eq. (1) is $\sin(\omega t+\theta_0)$. When the current peak appears at $t=t_{\text{peak}}$, the ac field in the simulation can be written as $\cos\omega t_{\text{peak}}=\sin(\omega t_{\text{peak}}+\pi/2)$. Because we assume in the theory that the electron returns to the target at $\omega t=2n\pi$, if the modulus of $\omega t_{\text{peak}}+\pi/2$ by 2π is n, the fixed point can be determined by $\theta_0=\omega t_{\text{peak}}+\pi/2-2n\pi$. For the measurement of the fixed point in this way, the current peak was picked up usually after 10–20 oscillations, which were enough to saturate the phase θ_0 (not the current itself). Note that the saturation of the current itself takes much longer than that. For the yield (δ) of the secondary electrons, we used[14,15,15] $\delta=\delta_{\max}sx/(s-1+x^2)$, where $x=E_i/\hat{E}$. Here, E_i is the energy of an incident electron, and s and $\hat{E}$ are empirically adjustable parameters. In our simulations, we set $s=1.35$ and $\hat{E}=318$ eV. For these choices, the number of electrons proliferated by the multipactor for most of the cases. Figure 6 is one example of such an electron avalanche.

III. EFFECTS OF THE ENERGY SPREAD OF THE SECONDARY ELECTRONS

In the previous section, we studied the behavior of the fixed point when the emission energy of the secondary electron is constant. However, in the real target, the secondary electrons always have an energy spectrum with a finite width. The energy spread is a material property. For example, the empirical formulas of the secondary energy spectra for copper and stainless steel are well summarized in Ref. 14. In this section we investigate how the fixed point diagram changes when a small amount of energy spread is added to a given emission energy.[17] We assumed a block spectrum of the initial velocity ν as in Fig. 7. For this energy spread, θ_{k+1} [the phase at the $(k+1)$th step] can be modified as follows:

$$\theta_{k+1}=\theta_k+\tau(\nu_k,\theta_k)-\tau(\nu_0,\theta_0), \tag{18}$$

where $\nu_k=\nu_0+\delta\nu_k$. The phase θ_{k+1} in Eq. (18) differs slightly from that used in the previous section in the middle term, where the flight time of the electron is now a function of ν as well as θ. From the fixed point (4), it can be verified that the order of $\delta\nu$ is $\sim\Delta$. Thus, it is reasonable to expand Eq. (18) up to the second order of $\delta\nu$ as well as Δ. Then the approximated equation looks like

$$\theta_{k+1}=\theta_k+\Delta_k\tau_0'+\delta\nu_k\partial_\nu\tau_0+\tfrac{1}{2}\Delta_k^2\tau_0''+\Delta_k\delta\nu_k\partial_\nu\tau_0'+\tfrac{1}{2}\delta\nu_k^2\partial_\nu^2\tau_0, \tag{19}$$

where the prime means the derivative in terms of θ as before. From Eq. (19), the mapping from Δ_k to Δ_{k+1} becomes

$$\Delta_{k+1}=\Delta_k(\bar{b}+a\Delta_k)+s, \tag{20}$$

where $\bar{b}=b+\delta\nu_k\partial_\nu\tau_0'$ and $s=\delta\nu_k\partial_\nu\tau_0+\delta\nu_k^2\partial_\nu^2\tau_0/2$. Here,

$$\left.\frac{\partial^2\tau}{\partial\nu\,\partial\theta}\right|_{\nu_0,\theta_0}=-\frac{2n\pi\sin\theta_0(1-\epsilon\partial_\nu\tau_0-\tau_0')}{(\nu_0-2n\pi\epsilon)^2}. \tag{21}$$

Equation (20) takes almost the same form as Eq. (12). The stability of the single bunch state is determined by the coefficient b, so its modification by the energy spread gives a small uncertainty to the first bifurcation point. The s-term changes slightly the equilibrium value of Δ, but it does not influence significantly the stability. Instead, it gives the phase spread to the fixed point θ_0.

Figure 8 shows the modified bifurcation diagram for $\nu=0.2\pm0.01$ and $\nu=0.2\pm0.03$ obtained from direct iteration of Eq. (20). The PIC simulation results are overlapped for several ϵ values, which show good agreement up to ϵ of 0.32. Beyond that the mapping equation (20) fails since it

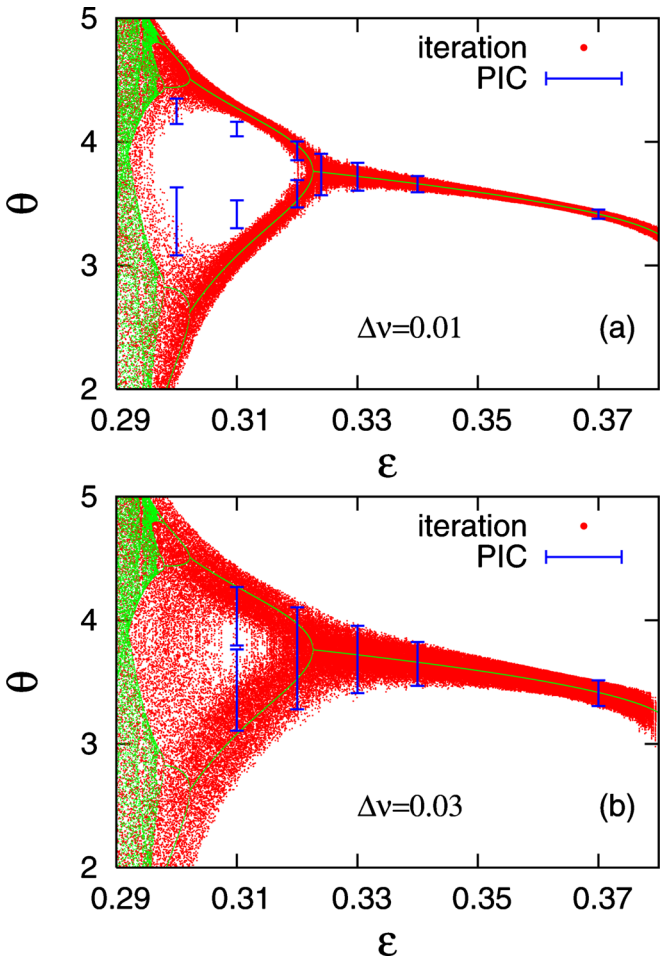

FIG. 8. (Color online) The bifurcation diagram for nonzero velocity spread of the secondary electrons for (a) $\Delta\nu$=0.01 and (b) $\Delta\nu$=0.03. The error bars represent not actually any error, but the duration of each current pulse measured from the PIC simulations. Note that, for zero-energy spread, the current pulses are narrow peaks as in Fig. 5. However, in the energy-spread case, the current pulses have finite duration as in Fig. 9.

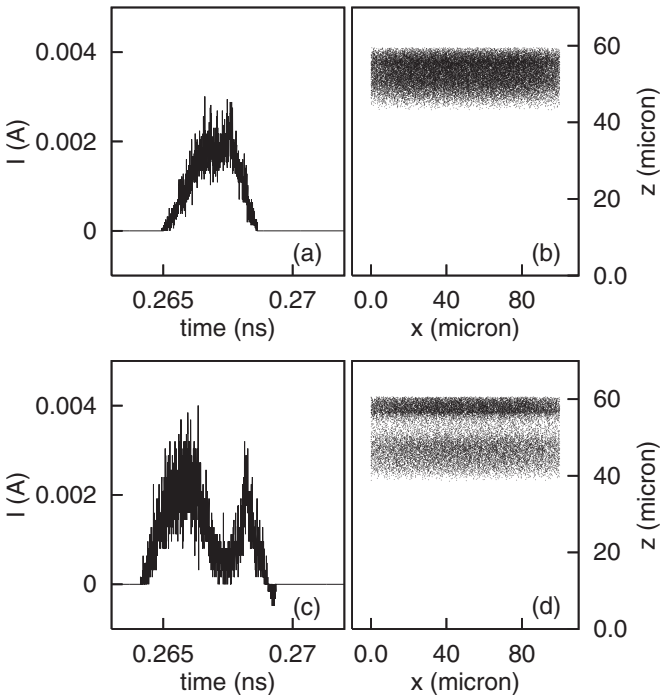

FIG. 9. The electric current and the particle distribution in the space for [(a) and (b)] ϵ=0.32 and [(c) and (d)] ϵ=0.31. The emission velocity is ν=0.2±0.03.

was derived for a small Δ only. The solid curves represent the bifurcation diagram when there is no emission energy spread. As can be expected, the two-period branch tends to smear out and higher-period branches are totally merged. For the second case in Fig. 8, where the velocity spread is about 15%, the parameter region for two-period branches is significantly reduced. The current throughout the emission target (Fig. 9) for ϵ=0.32, where a clear double bunching was observed for zero spread, now shows just a mere vestige of the bifurcation. For a clear observation of the double bunch in the energy-spread case, the dc field should be decreased more as in Fig. 8(b).

IV. CONCLUSION

Motivated by using the multipactor discharge as a generator of highly intense cold electron bunches, the dc-biased single-surface system has been theoretically studied. The dc-biased single-surface multipactor has received relatively little attention since the dc biasing is not a common configuration in generic rf systems. When the rf system is to be operated in the regime of tens of gigahertz frequency, dc biasing becomes even more difficult. That is, to keep the high quality factor of the rf resonator, the insulation gap to sustain the dc bias cannot be large enough. To solve this kind of problem, we suggested the photonic crystal structure in our previous work.

For the practical use of the dc-biased system, the behavior of the multipactor should be parametrized under diverse environments of the dc and ac fields and the secondary emission. In this paper we investigated the conditions for the phase lock of the electron bunch, the bifurcation, and the effects of the velocity spread of the secondary electrons. To summarize those works, first we found a quadratic function, which maps a perturbation to the fixed point at a given cycle to that in the next cycle. Here, the fixed point means an initial phase of secondary electrons relative to the ac field such that the next secondary electrons are also emitted with the same phase, repeatedly adding up to the monophased bunch. From the analysis of the mapping, the condition for the stable single bunch generation was revealed as a function of the ratio of dc and ac fields and the secondary emission velocity. Second the condition for the stable double bunch generation was also theoretically estimated in terms of the field strength and the secondary emission velocity. Third we added to the mapping the randomized term, from which the effects of the emission velocity spread could be explored. The bifurcated branches of the fixed point were merged to each other significantly by the velocity spread, while up to the double bunching those could be still observed for small velocity spreads. The velocity spread is a material property, so finding materials for small emission energy spread may be important in getting sharp electron bunches. Monte Carlo study for more realistic energy spread for copper and stain-

less steel is under progress. The theoretical results were verified by PIC simulations in wide ranges of the parameters, all of which showed good agreements. The parametrization of the single-surface dc-biased multipactor in this paper can be utilized for the experiments of the same system in the future.

ACKNOWLEDGMENTS

This research was supported by Basic Science Research Program through the National Research Foundation of Korea (NRF) funded by the Ministry of Education, Science and Technology (Grant No. 2010-0011429). This research was also supported by KERI.

[1]For a good review of the multipator discharge, see R. A. Kishek, Y. Y. Lau, L. K. Ang, A. Valfells, and R. M. Gilgenbach, Phys. Plasmas **5**, 2120 (1998), and references therein.
[2]F. Höhn, W. Jacob, R. Beckmann, and R. Wilhelm, Phys. Plasmas **4**, 940 (1997).
[3]H. C. Kim and J. P. Verboncoeur, Phys. Plasmas **12**, 123504 (2005).
[4]J. W. Noe, Nucl. Instrum. Methods Phys. Res. A **328**, 291 (1993).
[5]D. Proch, D. Einfeld, R. Onken, and N. Steinhauser, *IEEE Proceedings of the 1995 Particle Accelerator Conference* (IEEE, Piscataway, NJ, 1995), p. 1776.
[6]C. Chang, G. Z. Liu, J. Y. Fang, C. X. Tang, H. J. Huang, C. H. Chen, Q. Y. Zhang, T. Z. Liang, X. X. Zhu, and J. W. Li, Laser Part. Beams **28**, 185 (2010).
[7]C. Chang, H. J. Huang, G. Z. Liu, C. H. Chen, Q. Hou, J. Y. Fang, X. X. Zhu, and Y. P. Zhang, J. Appl. Phys. **105**, 123305 (2009).
[8]J. A. Nation, L. Schachter, F. M. Mako, L. K. Len, C.-M. Tang, and T. Srinivasan-Rao, Proc. IEEE **87**, 865 (1999).
[9]W. J. Gallagher, IEEE Trans. Nucl. Sci. **26**, 4280 (1979).
[10]E. F. Vance, J. Appl. Phys. **34**, 3237 (1963).
[11]V. Semenov, V. Nechaev, E. Rakova, N. Zharova, D. Anderson, M. Lisak, and J. Puech, Phys. Plasmas **12**, 073508 (2005).
[12]S. G. Jeon, J.-I. Kim, S.-T. Han, S.-S. Jung, and J. U. Kim, Phys. Plasmas **16**, 073101 (2009).
[13]S. Riyopoulos, Phys. Plasmas **14**, 112101 (2007).
[14]M. A. Furman and M. T. F. Pivi, Phys. Rev. ST Accel. Beams **5**, 124404 (2002).
[15]J. R. M. Vaughan, IEEE Trans. Electron Devices **36**, 1963 (1989).
[16]J. J. Scholtz, D. Dijkkamp, and R. W. A. Schmitz, Philips J. Res. **50**, 375 (1996).
[17]S. Riyopoulos, D. Chernin, and D. Dialetis, Phys. Plasmas **2**, 3194 (1995).